Solution of protein crystallographic structures by high-pressure cryocooling and noble-gas phasing

Chae Un Kim, Quan Hao and Sol M. Gruner

Solution of protein crystallographic structures by high-pressure cryocooling and noble-gas phasing

Chae Un Kim,[a,b] Quan Hao[b] and Sol M. Gruner[a,c,d]*

[a]Field of Biophysics, Cornell University, Ithaca, NY 14853, USA, [b]MacCHESS, Cornell University, Ithaca, NY 14853, USA, [c]Cornell High Energy Synchrotron Source (CHESS), Cornell University, Ithaca, NY 14853, USA, and [d]Physics Department, Cornell University, Ithaca, NY 14853, USA

Correspondence e-mail: smg26@cornell.edu

Room-pressure flash-cryocooling of protein crystals is the standard way to reduce radiation damage during data collection. Typically, it is necessary to find cryoprotection conditions by trial and error, a process that is not always successful. Recently, a new method, high-pressure cryocooling, was developed that does not require penetrative cryoprotectants and typically yields very high quality diffraction. Since this method involves helium gas as a pressurizing medium, it was of great interest to see whether the method could be extended to diffraction phasing by the incorporation of heavy noble gases such as krypton. A modified Kr–He high-pressure cyrocooling procedure is described wherein crystals are first pressurized with krypton gas to 10 MPa for 1 h. The krypton pressure is then released and the crystals are repressurized with helium over 150 MPa and cooled to liquid-nitrogen temperatures. Porcine pancreas elastase (PPE; 240 residues, 26 kDa) was selected as a test case for this study. Excellent diffraction was achieved by high-pressure cryocooling without penetrating cryoprotectants. A single 0.31 occupied krypton site in a PPE molecule [Bijvoet amplitude ratio ($\langle|\Delta F|\rangle/\langle F\rangle$) of 0.53%] was successfully used for SAD phasing at 1.3 Å. This method has the potential to greatly simplify obtaining protein structures.

1. Introduction

In X-ray crystallography, only the intensities of the diffraction reflections can directly be measured and the relative phase information is lost. This is the well known phase problem of X-ray crystallography. Various methods have been developed over the years to solve the phase problem (Dauter, 2006). The multiple isomorphous replacement (MIR) method was used to solve the first protein structures. However, it requires multiple crystals which have different kinds of heavy atoms as isomorphous derivatives. Furthermore, nonisomorphism between the crystals is very often a limitation. With the advent of intense and tunable synchrotron-radiation sources, methods based on the anomalous scattering that occurs when the scattered X-ray energy is near an absorption edge have become very popular. The multiple-wavelength anomalous diffraction (MAD; Hendrickson, 1999) method requires the collection of several complete sets of data at different carefully tuned energies spanning the absorption edge of incorporated resonant scattering atoms. The multiple passes increase the likelihood that radiation damage degrades the quality of the crystal and limits the accuracy of the intensity measurements. In some cases, the protein has naturally occurring suitable resonant atoms such as Fe. In more common cases, the atom has to be added to the protein; for example, during expression by replacement of S-methionine

with Se-methionine. Alternatively, the crystal may have unique sites for binding of specific resonant scatterers, as for example with soaks in heavy-atom solutions or by exposure to pressurized xenon gas.

More recently, single-wavelength anomalous diffraction (SAD) has been utilized to solve structures (Shen *et al.*, 2006). SAD is an experimentally simpler version of MAD. SAD does not require accurate X-ray wavelength tuning and the radiation damage is less problematic because only a single complete data set is required. The phase ambiguity that naturally arises in SAD phasing can be successfully broken using the Sim distribution (Hendrickson & Teeter, 1981), density modification (Wang, 1985) or direct methods (Fan *et al.*, 1984; Harvey *et al.*, 1998). Structures are increasingly being solved by SAD phasing, which is now of interest for high-throughput crystallography.

Since SAD phasing relies on a single data set, accurate and highly redundant intensity measurements are required, especially when weak anomalous scatterers such as sulfur are used (Ramagopal *et al.*, 2003). Assuming that a high-quality protein crystal is available, the next important step for accurate data collection is to find a suitable way to cryocool the crystal in order to minimize radiation damage. Protein crystals have most commonly been frozen by flash-cryocooling to near-liquid-nitrogen temperatures by immersion in cold gas or liquid at ambient pressure (Garman & Owen, 2006). There are two challenges with this procedure. Firstly, there is usually a requirement to find cryoprotectants to facilitate amorphous ice formation and reduce damage upon cryocooling. Finding suitable cryoprotectants is a trial-and-error process that is sometimes unsuccessful. Secondly, even if acceptable cryoprotectants can be found, the crystal quality is often degraded upon flash-cryocooling. This is manifested as an increase in the mosaic spread and a decrease in the observable diffraction resolution. This degradation in crystal quality limits the ability to phase the structure.

Recently, we have reported an alternative procedure, high-pressure cryocooling, for protein-crystal cryoprotection that does not require penetrative cryoprotectants (Kim *et al.*, 2005). Using high-pressure cryocooling, exceptionally high quality diffraction data were collected from several different kinds of protein crystals. Since this method involves the use of helium gas as a pressurizing medium, it is of interest to see whether the method could be extended to diffraction phasing by the incorporation of heavy noble gases such as krypton or xenon.

It has been reported that the noble gases krypton and xenon bind to several crystallized proteins (Schoenborn *et al.*, 1965; Tilton *et al.*, 1984; Schiltz *et al.*, 1994; Prangé *et al.*, 1998) and they have been used to solve protein structures (for a review, see Fourme *et al.*, 1999). Krypton (atomic number $Z = 36$) is lighter than xenon ($Z = 54$), but its K edge (14.3 keV, 0.87 Å) is readily accessible on most synchrotron beamlines, so krypton derivatization provides an opportunity to conduct anomalous diffraction experiments. Schiltz *et al.* (1997) reported that porcine pancreas elastase (PPE; 26 kDa) was successfully phased with a single half-occupied krypton by single isomor-

phous replacement with anomalous scattering (SIRAS). In the study, the anomalous signal was treated as an auxiliary source to improve the initial phase obtained by the isomorphous replacement signal. Later, krypton MAD phasing was successfully applied to the relatively small proteins myoglobin (17 kDa) and SP18 (18 kDa) (Cohen *et al.*, 2001). Those crystals were incubated in 2.76 MPa krypton gas for 2 min; the krypton pressure was then released and the crystals were flash-cryocooled in a nitrogen cold stream (100 K) at ambient pressure with the help of cyroprotectants (25% sucrose for myoglobin, 25% ethylene glycol for SP18). Four krypton-binding sites were found in myoglobin (occupancies of 0.68, 0.28, 0.17 and 0.08, respectively) and one krypton site was found in SP18 (occupancy of 0.42).

In this paper, porcine pancreas elastase (PPE) was selected as a test case for krypton SAD phasing. A half-occupied krypton in the PPE protein (Schiltz *et al.*, 1997) has an anomalous scattering strength of 1.9 e at its K absorption peak (14.3 keV). This anomalous strength in PPE (240 residues, 26 kDa) is predicted to give a small Bijvoet amplitude ratio ($\langle|\Delta F|\rangle/\langle F\rangle$, 380 water molecules in the PPE protein hydration layer were included in the calculation) of 0.86% (Hendrickson & Teeter, 1981). The solvent content of a PPE crystal is relatively low (35–40%), which makes density modification by solvent flattening less efficient (Ramagopal *et al.*, 2003). Here, we report a successful case of krypton SAD phasing of a PPE crystal, which had a single 0.31 occupied krypton site (estimated Bijvoet ratio of 0.53%) and 35% solvent content. The key feature that allowed this challenging PPE system to be phased was the very high quality diffraction obtained by the high-pressure cryocooling of the crystal.

2. Experimental

2.1. Materials and sample preparation

2.1.1. Crystallization of porcine pancreas elastase (PPE). Lyophilized PPE (catalog No. 20929) purchased from SERVA (Heidelberg, Germany) was used without further purification. Crystals were grown by the hanging-drop method by mixing 2 µl reservoir solution containing 30 m*M* sodium sulfate and 50 m*M* sodium acetate pH 5.0 with 2 µl of a 25 mg ml^{-1} protein solution in pure water (modified from Shotton *et al.*, 1968). Crystals appeared in a few days and crystals of dimensions $0.1 \times 0.1 \times 0.2$ mm were used for the Kr flash-cryocooling and Kr–He high-pressure cryocooling as described below.

2.1.2. Kr flash-cryocooling at ambient pressure. To study the krypton association/dissociation kinetics of PPE, crystal samples were prepared using a Xenon Chamber (Hampton Research, Laguna Niguel, CA, USA). Crystals were first coated with oil to remove excess mother liquor on the surface of the crystals and to prevent dehydration during gas pressurization. We previously investigated various oils and found that NVH oil (Hampton Research) works well with many proteins and protects against dehydration during gas processing. Hence, NVH oil was used in this study. Three NVH oil-

coated crystals were pressurized to the maximum pressure level of the gas chamber (4 MPa). After 10 min, the pressure was released in 20 s and the crystals were left in air for 5 s, 3 min and 9 min (named Kr10m_5s, Kr10m_3m and Kr10m_9m, respectively). The crystals were then flash-cryocooled at ambient pressure by plunging directly into liquid nitrogen. In parallel, an additional four crystals were pressurized to 4 MPa for 45 min, left in air for 5 s, 10 s, 3 min and 9 min and then flash-cryocooled in the same way (named Kr45m_5s, Kr45m_10s, Kr45m_3m and Kr45m_9m, respectively). The flash-cryocooling was carried out without adding penetrative cryoprotectants to compare the diffraction with that of the Kr–He high-pressure cryocooled crystals, which also do not contain additional penetrative cryoptotectants.

2.1.3. Kr–He high-pressure cryocooling. Details of the He high-pressure cryocooling process are described in Kim *et al.* (2005). Briefly, crystals are picked up in a cryoloop in a droplet of Hampton NVH oil. The purpose of the oil is to prevent dehydration of the crystal during the pressurization manipulations. As shown in Kim *et al.* (2005), crystals that are oil-coated and flash-cryocooled, as opposed to pressure-cryocooled, suffer considerably more cooling damage, *i.e.* the oil alone is not an adequate cryoprotectant. Although crystals with penetrative cryoprotectants can also be pressure-cryocooled, in our experience penetrative cryoprotectants are usually not needed with pressure cryocooling, so they were not used. The oil-coated crystals are loaded into the high-pressure cryocooling apparatus, which is then pressurized with helium gas to pressures in the 100–200 MPa range. Once at high pressure, a magnetic constraint is released and the crystals fall down a length of high-pressure tubing into a cold zone kept at liquid-nitrogen temperature. The helium pressure is released and the crystals are thereafter handled at ambient pressure, just as normal flash-cryocooled crystals for cryocrystallographic data collection.

The process for Kr–He high-pressure cryocooling is similar, but a little more complex. Firstly, three PPE crystals were carefully coated with NVH oil and loaded into the three pressure tubes of the apparatus, which were then connected to the gas compressor. The crystals were then pressurized with krypton gas to 10 MPa. After 1 h, the compressed krypton gas was released, liquid nitrogen was poured into the liquid-nitrogen bath of the pressure cryocooling apparatus and the crystals were re-pressurized with helium. After 90 s the helium pressure reached 155 MPa and the crystals were dropped into their respective tubes and cryocooled to liquid-nitrogen temperature at 155 MPa pressure. Overall, the time from krypton pressure release to cryocooling was about 200 s. The helium pressure was released 6 min after cryocooling and the crystals were transferred into cryocaps under liquid nitrogen for data collection. The three samples were named KrHe_1, KrHe_2 and KrHe_3, respectively.

2.2. Data collection

Diffraction data were collected at the Cornell High Energy Synchrotron Source (CHESS) on beamline F2 (beam diameter = 150 μm, ADSC Quantum 210 CCD detector). In all cases the detector face was perpendicular to the incident beam (2θ value of zero). All data were collected at 110 K (N_2-gas stream) and ambient pressure with an oscillation angle ($\Delta\varphi$) of $1.0°$ per image.

2.2.1. Data collection for Kr flash-cryocooled crystals. Diffraction data from seven Kr flash-cryocooled crystals were collected at 12.6 keV (0.9796 Å). The exposure time was 20–40 s and the distance between the crystal and detector (d) was 150–200 mm. A data set containing 100–120 frames was collected for structure determination from each crystal.

2.2.2. Data collection for Kr–He high-pressure cryocooled crystals. Diffraction data from three Kr–He high-pressure cryocooled crystals were collected at the absorption peak. In order to locate the 14.324 keV K edge of krypton, the monochromator crystals [Si(111)] were moved into the 14 keV region and calibrated using the L_I edge of gold at 14.353 keV. The PPE sample was then loaded onto a goniometer and a fluorescence scan was performed to find the absorption peak energy. Data were collected at the peak energy, 14.324 keV for the first two crystals (KrHe_1, KrHe_2) and 14.326 keV for the last one (KrHe_3), by the inverse-beam mode with a wedge of ten frames. The distance between the crystal and detector was 153–180 mm. The exposure time for each frame was 50–60 s. A total of 360 frames were collected from each crystal.

2.3. Data processing, phasing and model building

2.3.1. Kr flash-cryocooled crystals. Data were indexed, pre-refined, integrated, post-refined, scaled and merged with *HKL*2000 (Otwinowski & Minor, 1997). The initial structures were determined by the molecular-replacement method using *MOLREP* (Vagin & Teplyakov, 1997) from the *CCP*4 program suite (Collaborative Computational Project, Number 4, 1994) using the known protein coordinates 1c1m (Prangé *et al.*, 1998) from the PDB. The structures were then refined against the data sets with *REFMAC*5 (Murshudov *et al.*, 1997). As krypton occupancies and thermal B factors are highly correlated, the krypton occupancy was manually adjusted so that the refined thermal B factor of the Kr atom was close to the average thermal B factor of the crystallographically refined main-chain atoms.

2.3.2. Kr–He high-pressure cryocooled crystals. Data were indexed, pre-refined, integrated, post-refined, scaled and merged with *HKL*2000 (Otwinowski & Minor, 1997) as above but with the 'scale anomalous' flag to keep Bijvoet pairs separate. In the SAD phasing, the anomalous scattering substructure was initially solved and refined using the program *SAPI* (Hao *et al.*, 2003). The absolute configuration of the substructure was determined with *ABS* (Hao, 2004). The heavy-atom position was then input into *OASIS*-2004 (Wang *et al.*, 2004) for SAD phasing. Afterwards, density modification was performed using *DM* (Cowtan, 1994). Auto model building was performed with *ARP/wARP* (Perrakis *et al.*, 1999) and *REFMAC*5 (Murshudov *et al.*, 1997) was used for refinement.

Table 1
Summary of crystallographic statistics for the Kr flash-cryocooled crystals at ambient pressure.

Values in parentheses are for the last shell.

	Kr10m_5s	Kr10m_3m	Kr10m_9m	Kr45m_5s	Kr45m_10s	Kr45m_3m	Kr45m_9m
Wavelength (Å)	0.9796	0.9796	0.9796	0.9796	0.9796	0.9796	0.9796
Space group	$P2_12_12_1$	$P2_12_12_1$	$P2_12_12_1$	$P2_12_12_1$	$P2_12_12_1$	$P2_12_12_1$	$P2_12_12_1$
Unit-cell parameters (Å)							
a (Å)	50.4	50.5	50.2	49.3	50.0	50.3	50.4
b (Å)	58.1	58.2	57.9	57.3	57.7	57.8	58.1
c (Å)	74.9	74.8	74.8	74.1	74.5	74.4	75.0
Solvent content (%)	41	41	41	39	40	40	41
Mosaicity (°)	0.87	0.84	0.96	1.27	0.46	1.56	0.80
Resolution range (Å)	30–1.9 (1.97–1.9)	30–1.8 (1.86–1.8)	30–1.8 (1.86–1.8)	30–1.8 (1.86–1.8)	30–1.6 (1.66–1.6)	30–2.0 (2.07–2.0)	30–1.8 (1.86–1.8)
No. of observations	77092	93308	93121	89297	129576	51588	95105
No. of unique reflections	17551	20803	20973	19559	28401	14552	21175
Multiplicity	4.4 (2.7)	4.5 (3.9)	4.4 (3.7)	4.6 (4.2)	4.6 (3.6)	3.5 (2.6)	4.5 (4.0)
Completeness (%)	97.5 (93.2)	98.4 (95.5)	99.4 (97.0)	96.4 (95.7)	98.6 (99.9)	95.2 (89.4)	99.4 (95.6)
R_{sym} (%)	8.4 (27.3)	9.1 (40.6)	7.8 (28.8)	13.7 (42.9)	7.8 (24.4)	5.2 (20.5)	8.6 (23.7)
$I/\sigma(I)$	18.6 (3.7)	17.7 (2.9)	20.6 (3.3)	12.5 (2.5)	21.7 (4.8)	25.8 (5.0)	19.7 (4.5)
R value (%)	17.8	18.7	18.7	18.1	18.5	18.1	18.3
R_{free} value (%)	24.3	24.2	23.3	22.8	21.9	26.6	23.4
Average B factor (Å^2)	18.2	16.8	15.8	19.1	14.0	17.6	16.4
No. of water molecules	230	275	275	274	395	239	315
R.m.s. deviations from ideality							
Bond lengths (Å)	0.016	0.016	0.015	0.014	0.011	0.020	0.014
Angles (°)	1.5	1.5	1.5	1.5	1.3	1.8	1.4
Kr occupancy	0.47	0.13	0.09	0.43	0.32	0.20	0.05
Kr B factor (Å^2)	16.4	14.8	13.7	16.6	10.9	16.2	14.1

3. Results

3.1. Kr flash-cryocooled crystals and preliminary krypton occupancy study

The crystallographic data statistics for the Kr flash-cryocooled crystals are summarized in Table 1. The fact that crystal Kr45m_5s had almost the same occupancy (0.43) as crystal Kr10m_5s (0.47) confirms that the krypton binding to the PPE crystal under our experimental arrangement was complete within 10 min. The average krypton occupancy of crystal Kr10m_5s and Kr45m_5s was 0.45 and it appeared to be reasonable compared with the previously reported value of 0.49 at 5.6 MPa (Schiltz *et al.*, 1997). This occupancy (0.45) and the applied pressure ($P = 4$ MPa) were used to estimate the equilibrium constant (λ) of the krypton-binding reaction to PPE in the Langmuir isotherm: occupancy = $\lambda P/(1 + \lambda P)$ (Schiltz *et al.*, 1997). The calculated value (λ) was approximately 0.2 (MPa^{-1}). The Kr10m and Kr45m time series suggest that the krypton occupancy depends on the time for which crystals are left in a krypton-free environment: up to about 3 min, krypton diffused out from crystals relatively quickly. With longer times (from 3 to 9 min) the occupancy decreased more slowly.

These preliminary results were used to estimate the krypton occupancy in PPE crystals prepared by the Kr–He high-pressure cryocooling process described in §2.1.3. Firstly, the krypton pressurization of PPE crystals was long enough for saturation of the krypton-binding site. The maximum krypton occupancy at 10 MPa was estimated to be 0.67 using the Langmuir isotherm with the binding equilibrium constant $\lambda = 0.2$ (MPa)$^{-1}$. The ratio (0.37) of average krypton occupancy (0.165) of Kr10m_3m and Kr45m_3m to that (0.45) of Kr10m_5s and Kr45m_5s was used to roughly calculate the expected occupancy for the crystals left for 200 s before being high-pressure cryocooled. The estimated occupancy was approximately 0.25 or less.

3.2. Kr–He high-pressure cryocooled crystals and krypton SAD phasing

The crystallographic data statistics of the Kr–He high-pressure cryocooled crystals are summarized in Table 2. Since the anomalous scattering substructure was not clearly located in the KrHe_1 and KrHe_2 data, the krypton SAD phasing was performed with the KrHe_3 data set.

A single Kr-atom position was found and refined by *SAPI* using anomalous differences at 2.5 Å resolution with an R value of 30.1%. The absolute configuration of the substructure was determined with *ABS* and then the position was input into *OASIS*-2004 for SAD phasing at 1.3 Å. To evaluate the phase quality, an electron-density map (Fig. 1) was generated using *PyMOL* (DeLano, 2002). Density modification was performed using *DM* and the overall figure of merit increased from 0.5 to 0.695. Although the crystal KrHe_3 had very low solvent content (35%), density modification by solvent flattening seemed to improve the map quality. Therefore, the phases after *SAPI/ABS/OASIS*-2004/*DM* were used for model autobuilding in *ARP/wARP* with the default mode. After ten cycles of autobuilding, 219 residues out of 240 were found and docked in the electron density. The final R value was 27.0% with a connectivity index of 0.93. It was noticed in the electron-density map that most of the unassigned residues were distributed in the highly disordered regions adjacent to the solvent layer.

electronic reprint

In order to investigate the effect of resolution on the SAD phasing power, the 1.3 Å data set was cut off at resolutions of 1.5, 1.7, 1.8, 1.9, 2.0 and 2.5 Å and each data set was input into *OASIS*-2004 for SAD phasing. Although the figure-of-merit values at the cutoff resolutions were higher than the value at 1.3 Å, it turned out that the high-resolution data were essential for successful model autobuilding in *ARP/wARP*. At better resolution than 1.7 Å, *ARP/wARP* was able to find approximately 220 residues. However, *ARP/wARP* had difficulty in finding residues when the cutoff was raised to 1.8 Å and no residues were properly found with lower resolution data sets. Details of the results are summarized in Table 3.

To estimate the krypton occupancy by the same standard that was applied for the Kr flash-cryocooled crystals, the final refined structures of the Kr–He high-pressure cryocooled crystals were solved by the molecular-replacement method as described in §2.3.1. Since the anomalous signals were very weak in all cases, the signals were ignored in the model-construction process. As predicted, KrHe_1 and KrHe_2 had lower krypton occupancy (0.14 and 0.22, respectively) than KrHe_3 (0.31). Details of the refined structures are summarized in Table 2.

4. Discussion

It was shown that a single 0.31 occupied krypton site could successfully phase the PPE structure, which contains 240 residues (26 kDa). Since the estimated Bijvoet amplitude ratio ($\langle|\Delta F|\rangle/\langle F\rangle$) was only 0.53% and the solvent content was low (35%), the high-quality data obtained by Kr–He high-pressure cryocooling were essential for successful SAD phasing. The diffraction quality of PPE crystals prepared by Kr flash-cryocooling at ambient pressure and Kr–He high-pressure cryocooling was compared in terms of resolution limit and mosaicity (Fig. 2). The average resolution [cutoff $I/\sigma(I) \simeq 3.0$] and mosaicity of seven Kr flash-cryocooled crystals at ambient pressure (Table 1) were 1.7 Å and 0.97°, respectively. The average resolution [cutoff $I/\sigma(I) \simeq 3.0$] and mosaicity of three Kr–He high-pressure cryocooled crystals (Table 2) were 1.3 Å and 0.32°, respectively. This superior diffraction obtained by Kr–He high-pressure cryocooling was comparable to that of the PPE crystals prepared by successful flash-cryocooling at ambient pressure with 20% glycerol as a cryoprotecting agent (Mueller-Dieckmann *et al.*, 2004): the average resolution and mosaicity of nine PPE crystals prepared by the flash-cryocooling method with the cryoprotectant were 1.5 Å (or better) and 0.41°, respectively.

When very weak anomalous signals are involved, special efforts are often required in data collection to minimize the background scattering (Schiltz *et al.*, 1997). However, it should be mentioned that no such special efforts were taken during data collection for this study. Prior to the data collection, there was concern that the oil around the crystals might produce a significant background and hamper accurate signal measurement. However, accurate diffraction measurement was possible even in the presence of the oil background. We believe that the superior crystal diffraction achieved using

Table 2
Summary of crystallographic statistics for the Kr–He high-pressure cryocooled crystals.

Values in parentheses are for the last shell.

	KrHe_1	KrHe_2	KrHe_3
Wavelength (Å)	0.8656	0.8656	0.8654
Space group	$P2_12_12_1$	$P2_12_12_1$	$P2_12_12_1$
Unit-cell parameters (Å)			
a (Å)	50.2	46.7	46.6
b (Å)	58.2	57.9	57.7
c (Å)	74.6	73.9	73.7
Solvent content (%)	41	35	35
Mosaicity (°)	0.39	0.26	0.32
Resolution range (Å)	30–1.5	30–1.5	30–1.3
	(1.55–1.5)	(1.55–1.5)	(1.35–1.3)
No. of observations	433653	428805	614816
No. of unique reflections†	67826	61882	92573
Multiplicity†	6.4 (2.7)	6.9 (4.2)	6.6 (3.2)
Completeness (%)	99.9 (98.8)	99.5 (95.1)	98.0 (84.7)
R_{sym} (%)	7.6 (18.2)	6.7 (12.4)	5.3 (27.8)
$I/\sigma(I)$	28.2 (4.0)	35.7 (10.8)	42.7 (3.9)
$\langle|\Delta F|\rangle/\langle F\rangle$ (%)	2.44	2.20	3.19
$\langle|\Delta F|\rangle/\langle\sigma(\Delta F)\rangle$	0.57	0.84	0.84
R value (%)	18.7	20.7	21.6
R_{free} value (%)	22.5	24.3	23.5
Average B factor (Å^2)	14.1	13.5	14.0
No. of water molecules	435	361	387
R.m.s. deviations from ideality			
Bond lengths (Å)	0.009	0.010	0.008
Angles (°)	1.2	1.5	1.4
Kr occupancy	0.14	0.22	0.31
Kr B factor (Å^2)	10.5	10.06	10.15

† The Bijvoet pairs are kept separate in the statistics.

high-pressure cryocooling compensated for the background produced by the oil. Furthermore, it turned out that the oil coating is actually very useful in the krypton SAD phasing. As
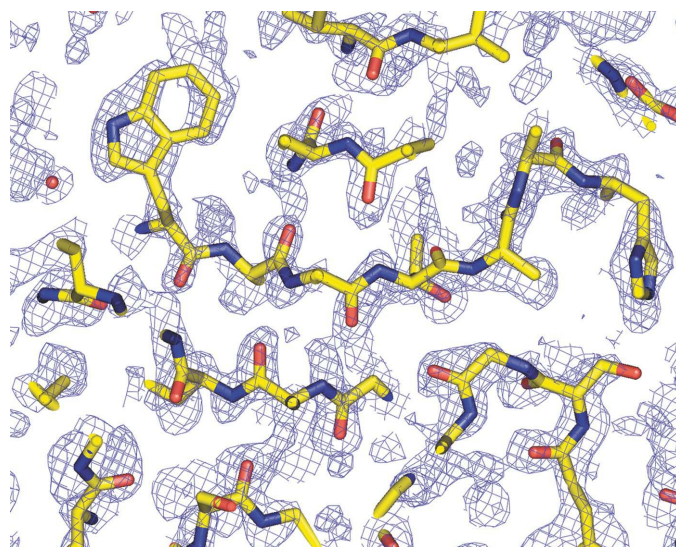

Figure 1
Electron-density map before density modification at 1.3 Å resolution. The final refined model solved by molecular replacement was superimposed for the map evaluation. The figure of merit is 0.5 and the map correlation coefficient calculated with the final refined density map is 0.58 for the main chain and 0.42 for side chains. The density map, contoured at the 1σ level, was prepared using *PyMOL* (DeLano, 2002)

the interaction between noble gases and other materials is the result of low-energy interactions (*e.g.* van der Waals forces), the solubility of xenon or krypton is significantly higher in oil than in pure water (Wilhelm *et al.*, 1977; Pollack *et al.*, 1989). The captured krypton in the oil during the Kr–He high-pressure cryocooling process produced a strong krypton fluorescence signal in the crystal scan step, which dramatically helped to locate the X-ray wavelength precisely at the krypton absorption peak. Moreover, owing to the higher affinity of krypton for oil than pure water, it is likely that krypton can stay in oil longer than in water. Therefore, oil may act as a krypton-buffering medium for the enclosed protein crystals when the outside compressed krypton gas is released. Indeed, the preliminary krypton occupancy study described in §3.1 showed that the krypton occupancy in PPE decreased relatively slowly over 9 min.

Capturing sufficient krypton during Kr–He high-pressure cryocooling seemed to be challenging. Since bulk krypton is in a solid phase at liquid-nitrogen temperature and solid krypton in the apparatus would hamper removal of the pressure-cryocooled crystals from the pressure tubings, the krypton pressure was released before filling the liquid-nitrogen bath. Limitations with the existing apparatus regarding the time it took to vent krypton and then pressure with helium meant that the crystals were exposed to low krypton partial pressure (0.1 MPa or less) for about 200 s before being high-pressure cryocooled. Even with the buffering effect of the oil, considerable krypton seemed to escape as soon as the krypton pressure was vented. The 200 s time interval was limited by the

time required to cryocool the sample assembly to liquid-nitrogen temperature (about 80 s) and the time to increase the helium pressure to over 100 MPa for the cryoprotection effect (about 80 s). With our existing apparatus, these two processes could not be performed at the same time. However, simple machine modifications would allow the entire pressurization and cryocooling process to occur in less than about 90 s. In this case, the krypton occupancy in PPE would be likely to be higher than the current estimated value of 0.25.

It should be emphasized that the estimated occupancy value is not the upper limit of the actual krypton occupancy. In the Kr flash-cryocooling, the krypton-containing crystals are exposed to air, *i.e.* a krypton-free environment. In contrast, in the Kr–He high-pressure cryocooling process, crystals are left in the pressure tubings that are partially filled with krypton gas even after the krypton pressure is released. In addition, although the solubility of helium in pure water is seven times smaller than that of krypton (Wilhelm *et al.*, 1977), considerable helium dissolves in water at 155 MPa.

We have not explored this quantitatively, but it might affect krypton solubility in water and its kinetics of protein association/dissociation. Indeed, one of the three Kr–He high-pressure cryocooled crystals showed higher occupancy (0.31) than the predicted upper limit value (0.25), suggesting some variability in our experimental setup.

In Kim *et al.* (2005), crystals were left under a high helium pressure for 25 min to be equilibrated. However, in this study the crystal was cryocooled within a few moments of application of a high helium pressure to limit the escape of krypton
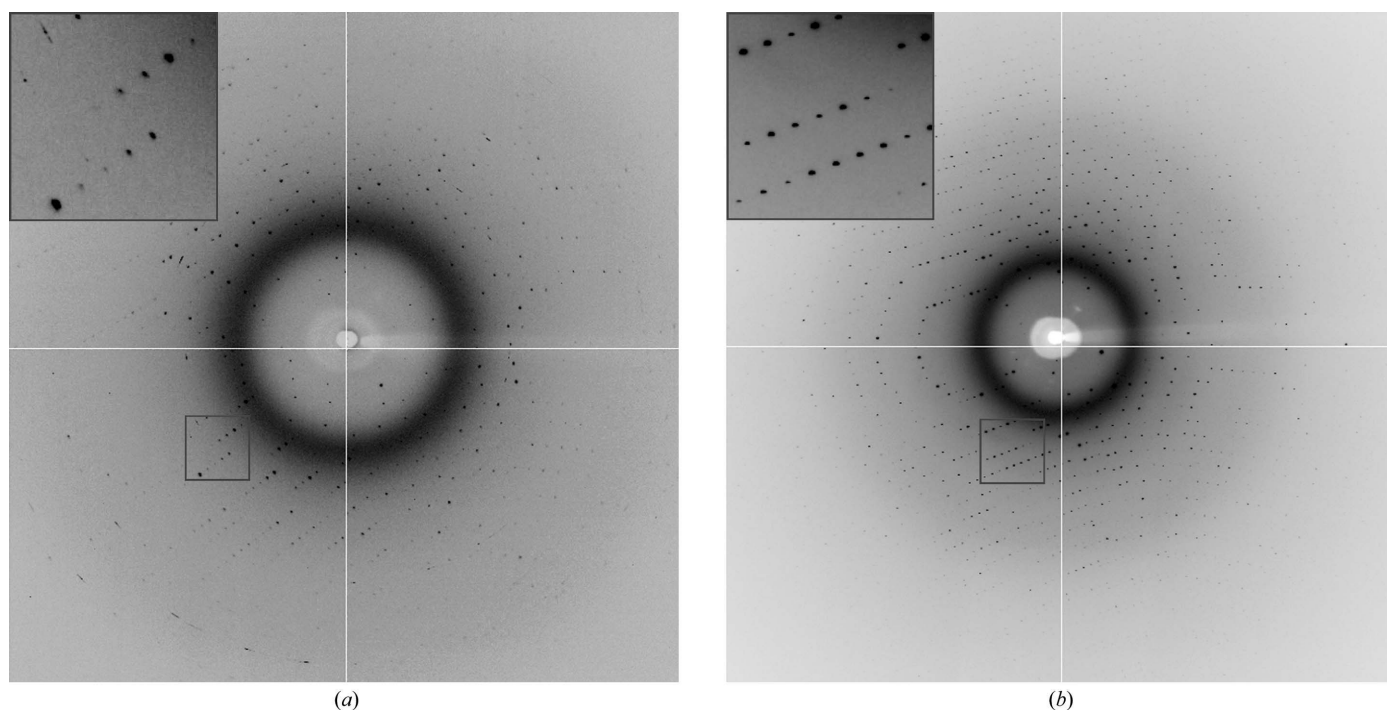

Figure 2
Diffraction images of PPE crystals. (*a*) Diffraction image of the crystal Kr10m_5s prepared by Kr flash-cryocooling at ambient pressure. The resolution limit [$I/\sigma(I) \simeq 3.0$] is around 1.8 Å and the mosaicity is 0.87°. The diffraction spots in the enlarged region look smeared. (*b*) Diffraction image of the crystal KrHe_3 prepared by Kr–He high-pressure cryocooling. The resolution limit [$I/\sigma(I) \simeq 3.0$] is around 1.2 Å and the mosaicity is 0.32°. The diffraction spots in the enlarged region look compact. This high-quality diffraction was obtained without adding any penetrative cryoprotectants.

Table 3
SAD phasing of KrHe_3 at different resolutions.

The map correlation coefficient was calculated with the $2F_o - F_c$ map of the final refined structure solved by molecular replacement.

Resolution (Å)	30–1.3	30–1.5	30–1.7	30–1.8	30–1.9	30–2.0	30–2.5
No. of unique reflections†	48640	32478	22469	18970	16203	13933	7252
$\langle|\Delta F|\rangle/\langle F\rangle$ (%)	3.19	2.11	1.74	1.64	1.56	1.52	1.38
$\langle|\Delta F|\rangle/\langle\sigma(\Delta F)\rangle$	0.84	1.07	1.25	1.34	1.40	1.45	1.59
FOM after *DM*	0.695	0.817	0.803	0.784	0.743	0.777	0.742
No. of residues found	219	224	227	34	0	9	0
No. of residues docked in sequence	219	224	227	9	0	0	0
Map correlation coefficient for main chain	0.71	0.79	0.74	0.70	0.64	0.60	0.40
Map correlation coefficient for side chain	0.56	0.66	0.59	0.56	0.51	0.47	0.32
R value (%)	27.0	21.8	21.5	23.7	23.0	19.7	18.5
Connectivity index	0.93	0.95	0.96	0.77	0.60	0.80	0.50

† The Bijvoet pairs are merged in the statistics.

inside the crystals. In order to investigate the structural perturbation caused by the Kr–He high-pressure cryocooling, the KrHe_3 structure solved by molecular replacement was compared with the room-temperature structure (PDB code 1c1m). The superposition of the two structures shows little difference: the r.m.s. deviation between the C^α backbone atoms in the two structures is 0.413 Å and the r.m.s. deviation between all atoms is 0.458 Å. The major structural deviation was observed in the floppy loop regions. Therefore, it is believed that in this case Kr–He high-pressure cryocooling resulted in relatively little perturbation of the structure.

Although the structural changes of PPE were small, significant differences in unit-cell parameters, especially along the *a* axis, were observed in KrHe_2 and KrHe_3 data. This unit-cell parameter variation contributed to the relatively lower solvent content (35%) of these two data sets. The reduced unit-cell volume of KrHe_2 and KrHe_3 might indicate that repacking of PPE molecules in the crystals occurred during high-pressure cryocooling. Further careful investigation will be required to reveal the correlation between this molecular rearrangement and the resultant diffraction quality.

Since Kr SAD phasing has been successful, our intention is to extend this method to the use of xenon gas. Xenon has many superior aspects for macromolecular crystallography compared with krypton. First, xenon has stronger protein binding (the polarizability of xenon is about twice as large as that of krypton; Schiltz *et al.*, 1997) so the occupancy of xenon in a protein is usually higher even when equilibrated at lower partial pressures. For example, the occupancy of xenon in PPE at 0.4 and 0.8 MPa are 0.71 and 0.93, respectively, whereas the occupancy of krypton in PPE at 5.6 MPa is only about 0.5 (Schiltz *et al.*, 1994, 1997). Another advantage is the fact that xenon seems to bind to proteins more slowly and in reverse diffuses out more slowly than krypton (Schiltz *et al.*, 1997; Cohen *et al.*, 2001). This suggests that it would be possible to obtain higher xenon occupancy during the high-pressure cryocooling process. Finally, xenon has much stronger anomalous signals even far from its *K* absorption edge (34.56 keV). For comparison, the $\Delta f''$ values of xenon at Cu *K*α (8 keV) and Cr *K*α (5.4 keV) are 7.4 and 11.8 e, respectively, whereas the $\Delta f''$ of krypton at its *K* absorption peak (14.3 keV) is only 3.8 e. Assuming the diffraction quality of a protein crystal is

the same as that of the PPE used for SAD phasing in this study, a single 0.5 occupied xenon can phase a protein as large as 250 kDa at Cu *K*α (8 keV) and 650 kDa at Cr *K*α (5.4 keV).

At longer wavelengths, the increasing anomalous strength of xenon competes with the accompanying increasing absorption and background, both of which limit the accuracy of the measurement of the anomalous signals. Therefore, the wavelength would have to be carefully selected to maximize the anomalous signal-to-noise. Mueller-Dieckmann *et al.* (2004) tested a xenon–PPE complex in the 0.80–2.65 Å wavelength range. They concluded that the optimal wavelength for anomalous signal data collection was between 2.1 and 2.4 Å, which indicates that xenon SAD phasing at longer wavelengths following high-pressure cryocooling might be generally applicable.

There is another factor that might enhance the benefits of data collection at longer wavelengths: the anomalous signal from S atoms originally present in proteins becomes more meaningful. The $\Delta f''$ of sulfur is 0.56 e at Cu *K*α (1.54 Å) and 1.14 e at Cr *K*α (2.29 Å) wavelengths. Indeed, sulfur anomalous signals have recently been used for SAD phasing (Hendrickson & Teeter, 1981; Wang, 1985; Dauter *et al.*, 1999; Liu *et al.*, 2000). In case the xenon anomalous signal itself is insufficiently strong for phasing, the native amino-acid sulfur anomalous signal at longer wavelengths can help the phasing process, where the xenon signal helps locate the S atoms as in the present krypton SAD phasing. As a trial to find additional potential anomalous scatterers, an anomalous difference map was created using *FFT* (Ten Eyck, 1973) with the phases calculated from the single 0.31 occupied krypton. As shown in Fig. 3, very strong density was found at the krypton site (the central density is higher than 100σ) and seven additional well confined sites were found around krypton at 3.6σ. To investigate the origin of these signals, the final refined model solved by the molecular replacement was superimposed on the density. We were able to assign six peaks out of the seven to S atoms (there are a total of 11 S atoms in the PPE structure). Two atoms out of six made a disulfide bond and their electron-density peaks were clearly distinguished. Since the anomalous strength of sulfur at the krypton peak (14.3 keV) is only 0.18 e, this is a remarkable result and reflects the quality of the diffraction produced by the high-pressure cryocooling.
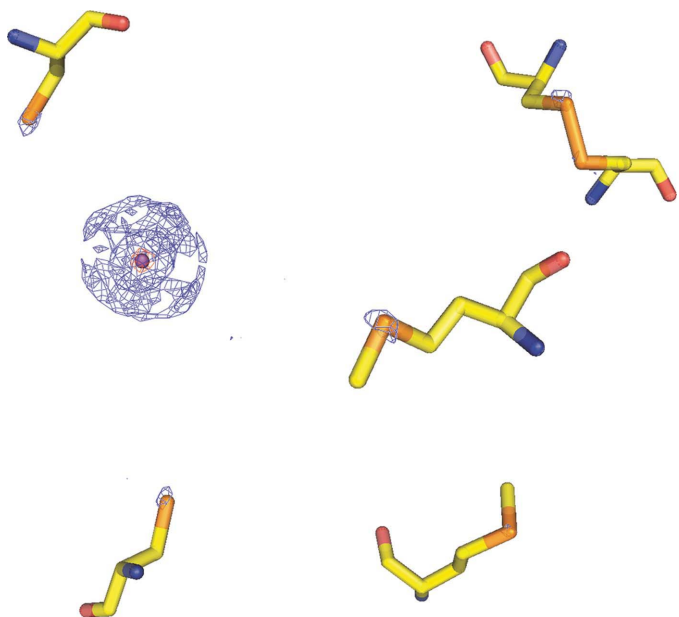
Figure 3
Anomalous difference map contoured at the 3.6σ level (blue) generated with the phases calculated from a single 0.31 occupied krypton. The final refined model obtained in the molecular replacement was superimposed to specify the origin of the peaks. Very strong density [central peak (red) contoured at 100σ] is found at the krypton site and six additional peaks are assigned to S atoms that are present in PPE. Two of them form a disulfide bond and their density peaks are clearly distinguished. The anomalous strength of sulfur at the krypton peak energy (14.3 keV) is only 0.18 e. The map was prepared using *PyMOL* (DeLano, 2002).

In summary, it has been shown that high-pressure cryo-cooling opens promising approaches for phasing. In Kr–He high-pressure cryocooling, crystals were successfully cryo-cooled without adding any penetrating cryoprotectants. The diffraction was of sufficiently high quality that the weak anomalous signal from a single 0.31 occupied Kr atom was sufficient for SAD phasing of the protein PPE, which has 240 residues (26 kDa). Since 30–50% of all proteins are expected to have binding sites for noble gases such as krypton and xenon (Stowell *et al.*, 1996; Fourme *et al.*, 1999), we believe that this method might become a very useful tool in many cases, eliminating the need for selenomethionine incorporation and the search for cryoprotectant conditions. This would be especially useful in cases where selenomethionine incorporation is difficult (*e.g.* many eukaryotic proteins) and for high-throughput crystallography.

References

Cohen, A., Ellis, P., Kresge, N. & Soltis, S. M. (2001). *Acta Cryst.* D**57**, 233–238.

Collaborative Computational Project, Number 4 (1994). *Acta Cryst.* D**50**, 760–763.

Cowtan, K. (1994). *Jnt CCP4/ESF–EACBM Newsl. Protein Crystallogr.* **31**, 34–38.

Dauter, Z. (2006). *Acta Cryst.* D**62**, 1–11.

Dauter, Z., Dauter, M., de La Fortelle, E., Bricogne, G. & Sheldrick, G. M. (1999). *J. Mol. Biol.* **289**, 83–92.

DeLano, W. (2002). *PyMOL.* DeLano Scientific, San Carlos, CA, USA.

Fan, H. F., Han, F. S., Qian, J. Z. & Yao, J. X. (1984). *Acta Cryst.* A**40**, 489–495.

Fourme, R., Shepard, W., Schiltz, M., Prangé, T., Ramin, M., Kahn, R., de La Fortelle, E. & Bricogne, G. (1999). *J. Synchrotron Rad.* **6**, 834–844.

Garman, E. F. & Owen, R. L. (2006). *Acta Cryst.* D**62**, 32–47.

Hao, Q. (2004). *J. Appl. Cryst.* **37**, 498–499.

Hao, Q., Gu, Y. X., Yao, J. X., Zheng, C. D. & Fan, H. F. (2003). *J. Appl. Cryst.* **36**, 1274–1276.

Harvey, I., Hao, Q., Duke, E. M. H., Ingledew, W. J. & Hasnain, S. S. (1998). *Acta Cryst.* D**54**, 629–635.

Hendrickson, W. A. & Teeter, M. M. (1981). *Nature (London)*, **290**, 107–113.

Hendrickson, W. A. (1999). *J. Synchrotron Rad.* **6**, 845–851.

Kim, C. U., Kapfer, R. & Gruner, S. M. (2005). *Acta Cryst.* D**61**, 881–890.

Liu, Z.-J., Vysotski, E. S., Chen, C.-J., Rose, J. P., Lee, J. & Wang, B.-C. (2000). *Protein Sci.* **9**, 2085–2093.

Mueller-Dieckmann, C., Polentarutti, M., Djinovic Carugo, K., Panjikar, S., Tucker, P. A. & Weiss, M. (2004). *Acta Cryst.* D**60**, 28–38.

Murshudov, G. N., Vagin, A. A. & Dodson, E. J. (1997). *Acta Cryst.* D**53**, 240–255.

Otwinowski, Z. & Minor, W. (1997). *Methods Enzymol.* **276**, 307–326.

Perrakis, A., Morris, R. & Lamzin, V. S. (1999). *Nature Struct. Biol.* **6**, 458–463.

Pollack, G. L., Kennan, R. P., Himm, J. F. & Carr, P. W. (1989). *J. Chem. Phys.* **90**, 6569–6579.

Prangé, T., Schiltz, M., Pernot, L., Colloc'h, N., Longhi, S., Bourguet, W. & Fourme, R. (1998). *Proteins*, **30**, 61–73.

Ramagopal, U. A., Dauter, M. & Dauter, Z. (2003). *Acta Cryst.* D**59**, 1020–1027.

Schiltz, M., Prangé, T. & Fourme, R. (1994). *J. Appl. Cryst.* **27**, 950–960.

Schiltz, M., Shepard, W., Fourme, R., Prange, T., de La Fortelle, E. & Bricogne, G. (1997). *Acta Cryst.* D**53**, 78–92.

Schoenborn, B. P., Watson, H. C. & Kendrew, J. C. (1965). *Nature (London)*, **207**, 28–30.

Shen, Q., Hao, Q. & Gruner, S. M. (2006). *Physics Today*, March, pp. 46–52.

Shotton, D. M., Hartley, B. S., Camerman, N., Hofman, T., Nyburg, S. C. & Rao, L. (1968). *J. Mol. Biol.* **32**, 155–156.

Stowell, M. H. B., Soltis, M., Kisker, C., Peters, J. W., Schindelin, H., Rees, D. C., Cascio, D., Beamer, L., Hart, P. J., Wiener, M. C. & Whitby, F. G. (1996). *J. Appl. Cryst.* **29**, 608–613.

Ten Eyck, L. F. (1973). *Acta Cryst.* A**29**, 183–184.

Tilton, R. F., Kuntz, I. D. & Petsko, G. A. (1984). *Biochemistry*, **23**, 2849–2857.

Vagin, A. & Teplyakov, A. (1997). *J. Appl. Cryst.* **30**, 1022–1025.

Wang, B.-C. (1985). *Methods Enzymol.* **115**, 90–112.

Wang, J.-W., Chen, J.-R., Gu, Y.-X., Zheng, C.-D., Jiang, F. & Fan, H.-F. (2004). *Acta Cryst.* D**60**, 1987–1990.

Wilhelm, E., Battino, R. & Wilcock, R. J. (1977). *Chem. Rev.* **77**, 219–259.